Slowly-attenuating P-SV Leaky Waves in a Layered Elastic Halfspace. Effects on the Coherences of Diffuse Wavefields

by

Antonio García-Jerez[12] and Francisco J. Sánchez-Sesma[3]

[1] Instituto Andaluz de Geofísica. Universidad de Granada. C/ Profesor Clavera, 12. 18071 Granada, Spain. Email: agjerez@ugr.es

[2] Also at Departamento de Física Teórica y del Cosmos, Universidad de Granada. 18071 Granada, Spain.

[3] Instituto de Ingeniería, Universidad Nacional Autónoma de México, CU, Coyoacán, 04510 D.F., Mexico.

Submitted to Wave Motion on 14th July 2014.

Accepted version.

Abstract

In the context of the classical real-frequency and complex-wavenumber (k) integral representation of the elastodynamic Green's function for a plane layered elastic medium, leaky modes are defined as those waves associated with complex-k poles in the P-SV integrands representing continuations of the higher Rayleigh modes below their cutoff frequencies. Nevertheless, for some types of models, the path of the leaky-mode poles through the complex plane (for varying frequency) can intercept the real k axis at particular frequencies, cancelling the complex character which was conferring to these wave the exponential decay as the horizontal distance increases. Starting from the Haskell–Harkrider formulation, the characteristics of these *slowly-attenuating* leaky waves and their excitation by surface forces are investigated. The conditions for existence and their frequency are evaluated for the particular case of an elastic layer over a halfspace. Some numerical simulations point to the detectability of these waves around the fundamental resonance of vertical S waves f_{S0} in standard frequency-domain observables defined for random elastic wavefields. These results provide new insights in the behavior of coherences of ambient seismic vibrations when a high velocity contrast exists.

Keywords: Rayleigh waves, leaky modes, Green's functions, diffuse wavefields

1. Introduction

The behavior of the elastodynamic Green's functions for a layered structure around the fundamental resonance of vertical S waves, f_{S0}, is an issue of importance in several branches of seismology and exploration geophysics. Even for simple ground models, the composition of the wavefield around f_{S0} may present a significant complexity. Maximum or infinite values in the ellipticity of the fundamental Rayleigh mode, the cutoff frequency of the first higher mode, the Airy phase of Love waves and a substantial increment in the relative power of P-SV body waves often occur near f_{S0} in simple models (e.g., Kono and Omachi [1], Tamura [2]). As a result, active and passive methods of seismic exploration based on analysis of Rayleigh waves may show perturbations in those frequencies (e.g., Tokimatsu [3], Ohori [4]).

On the other hand, the Green's functions between surface source and receiver are the key for advanced modelling of the background seismic wavefield (e.g., Sánchez-Sesma *et al.* [5], Lunedei and Albarello [6]). Thus, their precise description around f_{S0} is required for supporting or improving widespread ambient-noise techniques for estimation of ground resonances and amplifications of the seismic shaking (Nakamura [7]).

This article is devoted to the investigation of some properties of these Green's functions around f_{S0}. In particular, we study the role of a type of guided P-SV waves which appears in models with high velocity contrasts as the contributions of real-k poles in the leaky-modes branches.

In the extensive bibliography on computation of the complete elastodynamic Green's functions in layered media, several alternative schemes involving approximations of

their integral representations have been developed. Most of these methods evaluate integrals on the complex-frequency plane, on the complex wavenumber plane or on both of them (e.g. Gilbert [8], Ewing *et al.* [9], Haddon [10]). Analytic developments and numerical procedures have been used in different proportions. For example, body and surface wave contributions can be either computed together (e.g. Bouchon and Aki [11]) or calculated by well separated schemes resulting from the application of complex-plane integration methods. In the simplest versions of this latter approach (e.g. Wang and Herrmann [12]), Rayleigh waves arise as the contributions of real-k poles in the P-SV integrands, being evaluated from the Cauchy's residues theorem. On the contrary, body waves result from integrations along branch-lines laying on the real- and the imaginary-k axes. In principle, phase velocities of Rayleigh waves range, as much, between the S wave velocities of the top layer and the halfspace (e.g. Ben-Menahem and Singh [13]). The set of pole contributions and the path of the branch-line integrals to be evaluated are different for other choices of the integration contour.

In this work, we use real- and complex-wavenumber formulations to study a type of *trapped* P-SV wave system occurring at particular frequencies in some structures with sharp velocity increase with depth. The nature and the conditions for existence of these guided waves, which behave as Rayleigh-like waves spreading faster than β_N, are analyzed. They represent a limit situation appearing within broader spectral bands at which P-SV body waves generated by surface loads spread with high power at large horizontal distances. We show that these arrivals can be better incorporated in the calculations of Green functions in terms of leaky-modes poles. In fact, they correspond to isolated real-k points of the leaky-mode $k(\omega)$ paths, representing waves that attenuate slowly in the radial direction due to the cancellation of the imaginary component of k. No radiation of S waves into the halfspace occurs at these poles. We will use numerical examples to show that these waves can produce detectable effects in two frequency-domain observables defined in ambient noise seismology: the SPAC coefficient and the f-k power spectrum (Aki [14], Lacoss *et al.* [15]). The usual interpretation of these methods, based on the predominance of surface waves, fails in these specific conditions and frequency bands. Full-wavefield computations are then required.

Next, we derive useful conditions to locate these anomalous real-k poles in the Green's function integrand for a layered halfspace, as well as the main properties of the associated waves. After stating the connection between these poles and the leaky-mode formalism (Section 3), the frequencies and velocities of the slowly-attenuating leaky waves are computed for the case of a single layer (Section 4). The effects in ambient noise seismology methods are assessed in Section 5, and finally, some published experiments in which these waves may have played an important role are discussed in Section 6.

2. Fast P-SV guided waves in a layered elastic halfspace

We analyze a type of poles which occasionally arise in a classic representation of the frequency-domain Green's function in terms of integrals on the horizontal (radial) wavenumber k. Consider N-1 parallel elastic layers overlying an elastic halfspace, with α_m, β_m, ρ_m and h_m representing the P- and S-wave velocities, the mass density and the thickness of the m-th medium ($h_N = \infty$). A concentrated impulse force is applied at the origin of coordinates $\mathbf{x} = 0$, in the free surface. The force acts either in the vertical direction (subscript $j = z$, with Z axis is directed downwards) or radially towards the

point with cylindrical coordinates $(r,\theta,0)$ ($j = r$). Then, the Fourier-transformed vertical and radial displacements at point (r,θ,z) due to PSV-type (in-plane) waves are called Green's functions $G_{zj}^{PSV}(r,z;0;\omega)$ and $G_{rj}^{PSV}(r,z;0;\omega)$, respectively. These quantities can be first expressed in terms of an integral on k (real and positive for now) as follows:

$$G_{zz}^{PSV}(r,z;0;\omega) = i\int_0^\infty \frac{g_{zz}(\omega,k,z)}{F_R(\omega,k)} J_0(kr)dk \tag{1}$$

$$G_{rz}^{PSV}(r,z;0;\omega) = \int_0^\infty \frac{g_{rz}(\omega,k,z)}{F_R(\omega,k)} J_1(kr)dk \tag{2}$$

$$G_{zr}^{PSV}(r,z;0;\omega) = i\int_0^\infty \frac{g_{zr}(\omega,k,z)}{F_R(\omega,k)} J_1(kr)dk \tag{3}$$

$$G_{rr}^{PSV}(r,z;0;\omega) = i\int_0^\infty \frac{g_{rr}(\omega,k,z)}{F_R(\omega,k)} \left[J_0(kr) - J_2(kr)\right]dk\,, \tag{4}$$

where $J_n(\cdot)$ stands for the Bessel function of first kind and order n. For any contribution (ω, k), the boundary conditions of no upgoing energy and no inhomogeneous waves with unbounded amplitude are fulfilled inside the halfspace. Explicit expressions of the integrands were given by Harkrider [16] as well as the rest of the components of the P-SV Green's tensor (for arbitrary source direction and receiver position), which can be easily formed by linear combination of the four basic integrals (1-4).

In this framework, Rayleigh waves appear naturally as (real-ω, real-k) roots of the denominator F_R causing simple poles in the integrands, as described in the earlier work of Haskell [17], Eq. 2.21. As it is well known, for any ground model and frequency, there is, at least, one root of F_R (the fundamental mode) and the maximum velocities of these Rayleigh waves (including higher modes) are bounded by the halfspace S wave velocity β_N. Nevertheless, as will be shown in Sections 3 and 4, particular real-ω real-k pairs solving $F_R = 0$ can be found for k smaller than ω/β_N (i. e. corresponding to horizontal phase velocities greater than β_N). Following Harkrider [16], the full expression of F_R can be shortened to $F_R = NK - LM$, where the following definitions have been used:

$$\begin{aligned}
K &= \gamma_N \eta_{\alpha_N} A_{12} + (\gamma_N - 1)A_{22} - \frac{\eta_{\alpha_N} A_{32} - A_{42}}{\rho_N c^2} \\
L &= \gamma_N \eta_{\alpha_N} A_{11} + (\gamma_N - 1)A_{21} - \frac{\eta_{\alpha_N} A_{31} - A_{41}}{\rho_N c^2} \\
M &= -(\gamma_N - 1)\, A_{12} + \gamma_N \eta_{\beta_N} A_{22} + \frac{A_{32} + \eta_{\beta_N} A_{42}}{\rho_N c^2}
\end{aligned} \tag{5}$$

$$N = -(\gamma_{\mathrm{N}} - 1)\,\mathrm{A}_{11} + \gamma_N \eta_{\beta_{\mathrm{N}}} \mathrm{A}_{21} + \frac{\mathrm{A}_{31} + \eta_{\beta_{\mathrm{N}}} \mathrm{A}_{41}}{\rho_{\mathrm{N}} c^2}.$$

A represents the product of the Haskell's layer matrices (Haskell [17] or e.g., Eqs. 3.185 and 3.190c in Ben-Menahem and Singh [13]), $c = \omega/k$, $\gamma_m = 2\beta_m^2/c^2$, $\eta_{\alpha_m} = \frac{-i}{k}\sqrt{k^2 - k_{\alpha_m}^2}$, $\eta_{\beta_m} = \frac{-i}{k}\sqrt{k^2 - k_{\beta_m}^2}$, $k_{\alpha_m} = \omega/\alpha_m$, $k_{\beta_m} = \omega/\beta_m$.

We can now study those zeroes of F_R due to the simultaneous fulfillment of the equations $K = 0$ and $L = 0$ with $\beta_{\mathrm{N}} < c < \alpha_{\mathrm{N}}$. As it has been demonstrated in Appendix A, any solution (ω_p, k_p) of this system corresponds to a wave with the following properties:

i) the particle motion at surface follows an elliptical trajectory with imaginary ellipticity ratio $\dot{u}/\dot{w} = -M/N$ (i. e. $\pm\pi/2$ phase lag between horizontal and vertical components, just as regular Rayleigh waves);

ii) the wavefield at the halfspace consists of a pure inhomogeneous P wave with exponentially decaying amplitude as depth increases;

iii) its excitation by a surface force is given by the Rayleigh-wave *medium response* (Harkrider [16]): $A = -iG\left[(\partial K/\partial k)_{\omega_p} - (M/N)(\partial L/\partial k)_{\omega_p}\right]^{-1}$, where G follows Haskell`s [17] definition (Appendix A).

In the illustrative case of a single plane elastic layer overlying a halfspace (N = 2) with $\beta_2 > \beta_1$, it is clear from ii) that the wavefield components at ω_p can be decomposed in terms of upgoing and downgoing P and S waves as sketched in Figure 1. P waves inside the layers can be either of homogeneous (Fig. 1a) or inhomogeneous type (Fig. 1b).

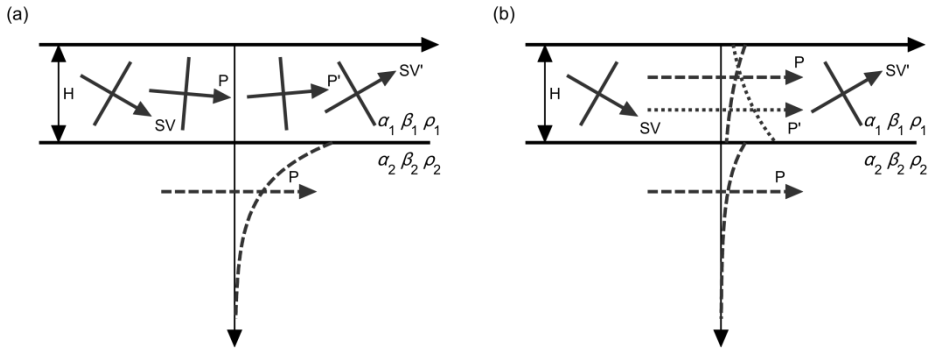

Figure 1. Diagram of the possible wave system components at (ω_p, k_p) in terms of upgoing and downgoing P and S waves or their inhomogeneous counterparts. (a) Case $c > \alpha_1$; (b) case $c < \alpha_1$. The amplitude of the S waves in the halfspace vanishes for this wave system.

3. Connection with the leaky-modes formalism.

The resolution of integrals (1-4) is often performed by extending the integral in *k* or/and in ω to the complex plane and subsequently deforming the integration contour in order to avoid passing through any zero of F_R. The contributions of these poles of the integrands are finally taken into account by summing the corresponding residues (Cauchy's theorem). In this section, the complex-*k* real-ω approach will be used. Several ways to solve these complex-variable integrals have been discussed in the literature (e.g., Ben-Menahem and Singh [13], Watson [18], Wang and Herrmann [12]). Major variations between methods lie in the different ways of defining the square roots in η_{α_N} and η_{β_N} in the complex plane because they cause branch-cut discontinuities in the integrand that have to be considered for choosing the integration contour. The simplest choice (e. g. Wang and Herrmann [12], Tamura [2]) consists in using the principal value of the square root and it has the advantage of keeping all the roots of F_R on the real *k* axis (Fig. 2), where their numerical computation is simpler. The branch-cut discontinuities of both $\sqrt{k^2-k_{\alpha_N}^2}$ and $\sqrt{k^2-k_{\beta_N}^2}$ when the radicands are negative reals produce jumps of the integrand on the whole imaginary axis as well as in the interval $[-k_{\beta_N}\ k_{\beta_N}]$ of the real axis.

As was noticed by Laster *et al.* [19], a weakness of this choice resides in the difficulties to evaluate some oscillatory events by means of the branch-cut integrals. These instabilities are related with the existence of complex-*k* roots of F_R at different Riemann sheets (i.e. appearing only under alternative definitions of signs in the roots of η_{α_N} and η_{β_N}) but still located close to the branch-cuts and occasionally on them. Anomalous poles of this type have been described in more detail by Surkov and Reshetnikov [20]. Then, the most convenient procedure to handle these cases is to reroute the branch-cuts and the lines of integration into the complex *k* region in such a manner that the integrand is a rapidly decaying function. As a result, residues at complex-*k* poles (leaky modes) have to be summed into the Green's function along with Rayleigh wave contributions. It is clear that the guided waves described in section 2 represent extreme cases of instability in the original branch-line integrals caused when the path of the leaky mode poles occasionally reaches the real axis on the integration contour (red circles in Fig. 2). Model 1 in Table 1, with ρ and *h* standing for mass density and layer thickness, can be used to illustrate this case. It is among the models used by Tuan *et al.* [21] for studying Rayleigh wave properties.

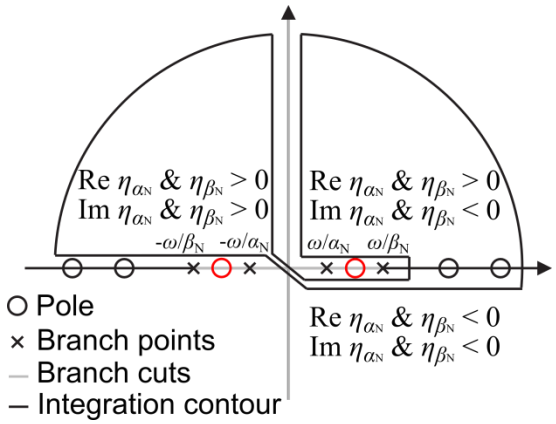

Figure 2. Possible integration path (thick black line) for the *P-SV* integrals in Eqs. (1-4) assuming that the principal value of the square roots is taken for evaluation of η_{α_N} and η_{β_N}. This choice of Riemann surface prevents for existence of poles at complex *k*'s. Branch-points and branch cuts are shown with X and gray lines, respectively. Black circles represent possible Rayleigh wave poles. Red circles represent possible high-velocity poles associated to the slowly-attenuating leaky waves studied here. An additional pole at $k = 0$ appears in the calculation of $G_{rr}^{PSV}(r,z;0;\omega)$ (Wang and Herrmann [12]). Cases Re[$k\eta_{X_N}$]<0 and Im[$k\eta_{X_N}$]<0, $X = \alpha, \beta$ fulfill the boundary conditions in the halfspace, wherein the amplitudes of P and S waves assumed to be proportional to $\exp(-i\omega t - ik\eta_{X_N} z)$.

Table 1. Example models presenting a pole in the P-SV integrand at $k_{\alpha_2} < k < k_{\beta_2}$

h (m)	α (m/s)	β (m/s)	ρ (g/cm^3)
Model 1			
50	663.3	200	2.0
∞	1370.1	$666.\widehat{6}$	2.7
Model 2			
25	1350	200	1.9
∞	2000	1000	2.5

To investigate the origin of these real poles, the scheme of branch-cut rerouting used by Laster *et al.* [19], Ben-Menahem and Singh [13] or Watson [18] is followed. Conjugation of the integrands is required to meet the definition of Fourier transform used in the first and second references. Therefore, the sign of η_{β_N} are changed in the region Im(k) > 0, 0 ≤ Re(k) < k_{β_N} as well as in the region Im(k) < 0, $-k_{\beta_N}$ < Re(k) ≤ 0, proceeding in a similar way for η_{α_N} (k, k_{α_N}). It sets the branch-cut discontinuities going *upwards* from k_{α_2} and k_{β_2}, as shown in Fig. 3c. Thus, the full integration path encompasses the first and second quadrants, going along the real axis through the second and fourth quadrants and encircling the branch-cuts in the first one (e.g., Ben-Menahem and Singh [13], p. 264, after complex conjugation). The additional complex-*k* poles exposed in the regions of the first quadrant with redefined η_{β_N} and/or η_{α_N} have

to be considered in the sum of residues. Due to the properties of F_R, each pole at k in the mentioned regions of the first quadrant has a counterpart located at $-k$ as well as two more roots at k^* and $-k^*$ located at lower Riemann sheets.

The contact of the path of leaky-mode poles with the real k axis at a particular frequency f_p has been shown by a green dot in Fig. 3c. The asterisks in that panel show the route of the leaky-mode branch obtained by continuation towards low frequencies of the first higher mode of Rayleigh waves. In order to keep the branch-cuts fixed while frequency varies, the complex horizontal slowness plane has been used in that figure instead of k. For Model 1, f_p lies very close to the resonance of vertical S waves $f_{S0} = \beta_1/(4h)$ at 1Hz and corresponds to phase and group velocities ($c = \omega/\mathrm{Re}[k]$, $c_g = d\omega/d\,\mathrm{Re}[k]$) of 874 m/s and 352 m/s, respectively. The separate evolution of the real and imaginary parts of these poles for varying frequency is shown in Figs. 3ab in terms of phase velocity and attenuation expressed in dB/km. The imaginary part of these roots produces the exponential decay of amplitude with distance, distinctive of the leaky modes. As was demonstrated in Section 2, the $\dot{u}/\dot{w}$ ratio for these waves becomes imaginary at f_p (same as for Rayleigh waves), with values of $\mathrm{Im}(\dot{u}/\dot{w})$ close to a local maximum and predominance of horizontal motion (Fig. 3d).

The comparison between medium response curves (Fig. 3e) shows that the leaky modes are much more excited around f_p ($\sim f_{S0}$) by a vertical load than the fundamental Rayleigh mode. This dominance is also illustrated by the synthetics waveforms of $G_{zz}^{PSV}(r,0;0;t)$ depicted in Fig. 4 after convolving with a 0.28s long parabolic pulse. The pulses associated with the leaky waves studied here are identified in Fig. 4b by applying a Gaussian filter $H(f)$ with central frequency f_p = 1Hz. For a filter parameter of about 10 (or larger), i.e. $H(f) = \exp\{-10\,[(f - f_p)/f_p]^2\}$, the spreading of the envelope of the filtered traces, which have been enlarged in amplitude, matches well the theoretical group velocity of the leaky mode.

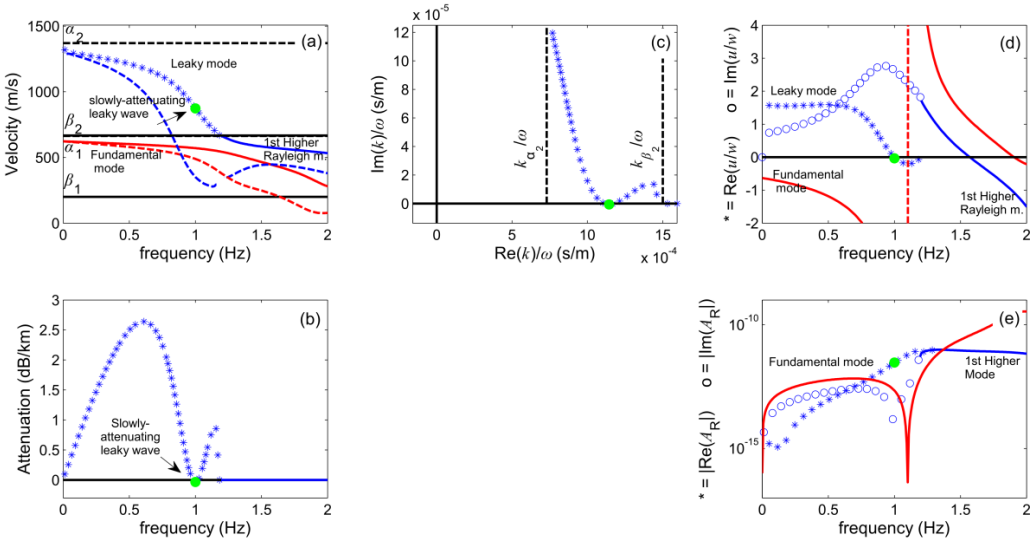

Figure 3. Leaky-mode poles (blue symbols) resulting from continuation of the first higher mode of Rayleigh waves below its cutoff frequency for the model in Table 1. The green dots show

values at f_p. (a) Phase (solid) and group (dashed) dispersion curves of the fundamental (red lines) and the first higher mode (blue lines) of Rayleigh waves. Blue asterisks represent leaky modes. (b) Attenuation of leaky waves as a function of the frequency calculated from Im[k]. Exponential attenuation appears neither at f_p nor for the Rayleigh mode. (c) Path of the leaky-mode pole through the complex- horizontal slowness plane (k/ω, with real ω) as frequency varies. The branch-cuts have been chosen going *upwards* from $k_{\alpha_2}/\omega = 1/\alpha_2$ and $k_{\beta_2}/\omega = 1/\beta_2$. (d) Horizontal-to-vertical ratio $\dot{u}/\dot{w}$ and (e) medium response for the leaky modes (symbols), the fundamental (red lines) and the first higher mode (blue lines) of Rayleigh waves.

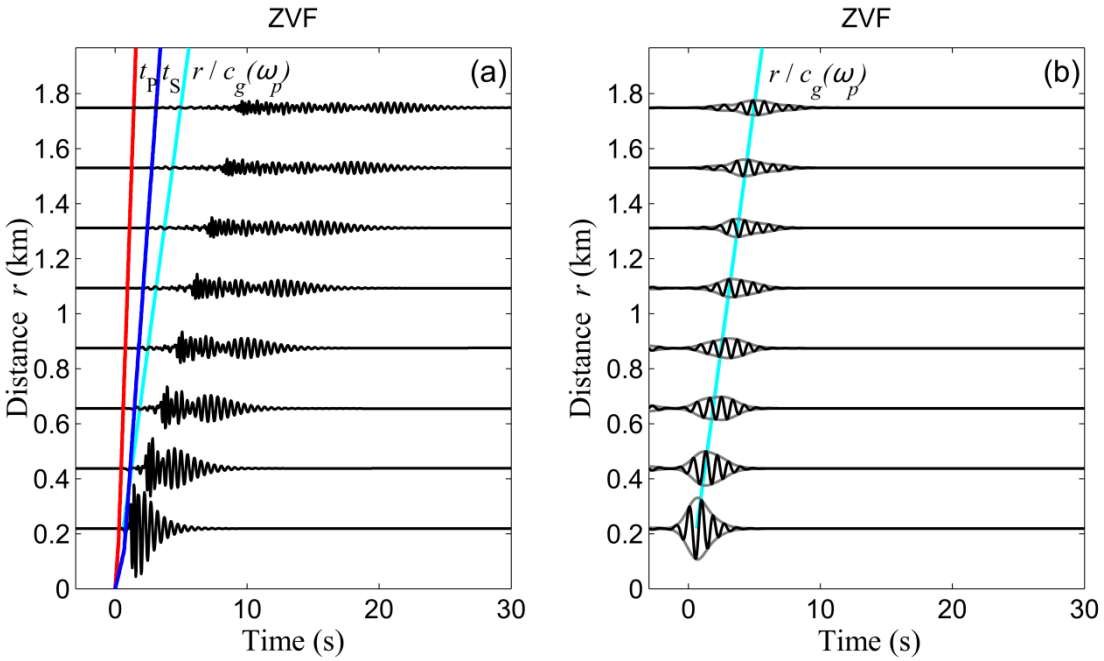

Figure 4. (a) Synthetic Green`s function $G_{zz}^{PSV}(r,0;0;t)$ for Model 1 (Table 1) calculated at several distances and convolved with a 0.28s long parabolic pulse. The first arrival time curves of P and SV waves are indicated with red and blue lines, whereas the cyan line shows the arrival time of the studied guided wave calculated from its group velocity $c_g(f_p)$ of 352 m/s (Fig. 3a). (b) G_{zz}^{PSV} functions after bandpass filtering around f_p = 1Hz and their respective envelopes. A Gaussian filter with bandwidth parameter 10 and subsequent rescaling have been applied.

4. Frequency and velocity of slowly-attenuating leaky waves for a layer-over-halfspace model.

The existence of slowly-attenuating leaky waves due to the simultaneous fulfillment of equations $K = 0$ and $L = 0$ and the determination of the frequency and velocity of these waves can be easily addressed by numerical procedures. For simple models consisting of a single layer overlying a halfspace, $K(c, k)$ and $L(c, k)$ depend on kh through trigonometric functions with arguments $k\eta_{\alpha_1}h$ or $k\eta_{\beta_1}h$. A suitable procedure based on eliminating the dependence on $k\eta_{\alpha_1}h$ between both equations is described in Appendix B. This step leads to a necessary condition for (c_p, k_p) with the form $\mathrm{X}\tan^2(k\eta_{\beta_1}h) + 2\mathrm{Y}\tan(k\eta_{\beta_1}h) + \mathrm{Z} = 0$, with X, Y and Z depending on c and on the model velocities and densities, which provides a family of tentative relationships *k(c)*

(note the multivalued character of the square root and function $\tan^{-1}$). Once $k(c)$ are inserted in any of the original equations, the problem is reduced to the numerical solving a single equation in the unknown c.

As it has been shown above, this type of guided waves may appear on the continuation of the first higher mode to lower frequencies as a leaky-mode curve. Thus, it is expected that the frequencies of these waves will be around the resonance frequency f_{S0}. To check this conjecture, f_p (if it exists) has been calculated for a representative set of models. We first fix the Poisson's ratio in the halfspace ν_2 at 0.3449 and the density contrast ρ_1 / ρ_2 at 0.7391 and vary β_1/β_2 and ν_1. These constants are taken from a previous work by Tuan *et al.* [21] devoted to studying the shape of the Rayleigh wave ellipticity. The (lowest) frequencies at which this slowly-attenuating leaky wave appears are shown in Fig. 5a. Next, ν_1 is fixed at 0.3449 and ν_2 is varied together with β_1/β_2, leading to the results shown in Fig.5b. The maximum deviations of the f_p values from f_0 are about $\pm 30\%$ in Fig. 5, though they are smaller for the most usual Poisson's ratios and β_1/β_2 below ~0.4. For most of the evaluated models, the wave system contains homogeneous P waves in the layer ($c > \alpha_1$), corresponding to the scheme in Fig. 1a. On the contrary, all the P waves are inhomogeneous for some models with high ν_1 and relatively low velocity contrast (i.e., large enough β_1/β_2), which have been marked with dots in Fig.5a. The anomalous poles studied here are absent for models in these grids with lower velocity contrast and higher Poisson's ratios.

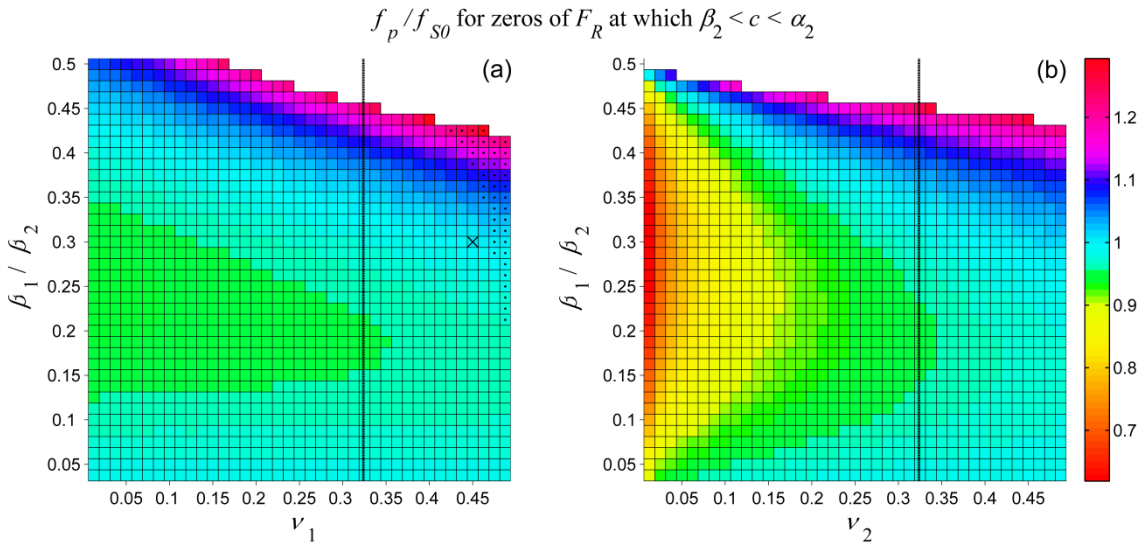

Figure 5. Lower frequency at which slowly-attenuating leaky waves exist for a set of models consisting of a layer overlying a halfspace. (a) f_p / f_0 for a constant $\nu_2 = 0.3449$; (b) same for a constant $\nu_1 = 0.3449$. A density ratio $\rho_1 / \rho_2 = 0.7391$ was used for all models. Dotted cells distinguish models for which all P waves are of inhomogeneous type (i.e., following the sketch in Fig. 1b). The X identifies Model 1 (Table 1). The intersection between both panels is shown with a vertical black line.

5. Effects on the coherences of diffuse wavefields

Even though the predominant role of surface waves in the seismic noise wavefield has been recognized in broad frequency bands and in most of the experimental situations, the composition of these vibrations around the resonance frequency f_{S0} is still a topic of current research in seismological engineering (e.g. Endrun [22]). This topic has essential

implications in seismic site effects evaluation and important consequences regarding the applicability of passive seismic methods of seismic exploration. These aspects have been mainly tackled from numerical and experimental points of view (e.g., Bonnefoy-Claudet *et al.* [23], Chávez-García *et al.* [24]).

Under the diffuse field approach (DFA), correlations of ambient noise can be directly connected with the elastodynamic Green's functions between surface source and receivers (Shapiro and Campillo [25]). As was shown by Yokoi and Margaryan [26], after a convenient normalization, the cross-spectra between pairs of ambient noise records defined by Aki [14] equal the imaginary part of the corresponding Green's functions in frequency domain. Taking advantage of this way of having experimental access to the Green's functions, the detectability of the slowly-attenuating guided waves described in Section 2 are investigated below. We pay attention to the effects of the complex wavefield composition around f_{S0} on two phase velocity estimators broadly used in ambient noise seismology: the SPatial Auto-Correlation coefficient and the conventional *f-k* power spectrum.

5.1. Effects on the vertical-component coherence

On the basis of the DFA, the coherence between vertical microtremor records at points $\vec{r}_1$ and $\vec{r}_2$ with interstation distance r (v-SPAC coefficient following Aki [14]), can be written, as

$$\rho_{1,2}(r,\omega) = \frac{\mathrm{Re}[C_{12}]}{\sqrt{C_{11}C_{22}}} = \frac{\mathrm{Im}[G_{zz}(r,0;0;\omega)]}{\mathrm{Im}[G_{zz}(0;0;\omega)]} \quad . \tag{10}$$

C_{jl} in (10) represents $\left\langle w^*(\vec{r}_l)w(\vec{r}_j)\right\rangle$, $\langle\cdot\rangle$ stands for average over a set of long enough time windows and $w(\vec{r}_j)$ is the Fourier transformed vertical motion at $\vec{r}_j$. Dependences of C_{jl}, w, and $\rho_{1,2}$ on ω are understood. The right hand side of Eq. (10) becomes $J_0(k'r)$ in frequency bands wherein a single k' (or horizontal velocity ω/k') dominates the vertical component. Although this case usually corresponds to the existence of a predominant mode of Rayleigh waves [14], the same functional behavior is expected at ω_p if slowly attenuating leaky modes are dominant contribution.

Figure 6a shows the results of a full-wavefield computation of $\rho_{1,2}(f)$ for Model 1 (Table 1) and r = 230 m. For this radius, a bump appears around f_p, approximately in the band 0.7-1.3 Hz, wherein leaky waves and the higher mode are expected to be the dominant contributions on the basis of the values of the medium responses (Fig. 3e). Features similar to this have been described in the literature and interpreted in terms of contribution higher Rayleigh modes (Roberts *et al*. [27], Asten [28], Ikeda *et al.* [29]). The apparent loss of correlation at 0.85 Hz is therefore an effect of the return to the fundamental-mode curve as the frequency decreases after a significant band dominated by leaky modes spreading with higher velocity.

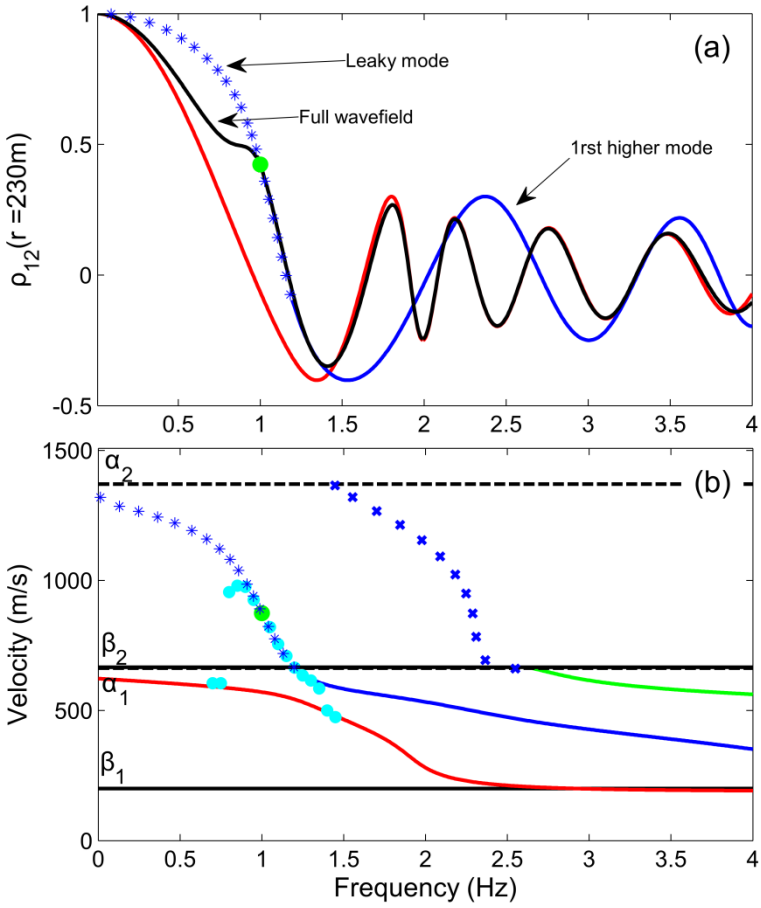

Figure 6. (a) Full-wavefield calculation of $\rho_{1,2}(230m)$ under the DFA for Model 1 in Table 1 (black line). Respective curves for the fundamental and first higher Rayleigh modes as well as for the leaky mode of interest are shown with red line, blue line and blue asterisks. (b) Rayleigh wave dispersion curves and leaky modes (asterisks and crosses). Cyan and green dots show velocities c' determined by fitting $\rho_{1,2}$ vs. r with a function $J_0(\omega r/c')$, as shown in Fig. 7.

To better assess the composition of the wavefield in this band and its effects on the SPAC curve, it should be useful to examine the coherences obtained for a range of interstation distances. Full-wavefield $\rho_{1,2}$ vs. r curves have been represented in Fig. 7 for 16 frequencies and subsequently fitted to the expression $J_0(\omega r/c')$. The optimum c' for each frequency has been represented with dots in Fig 6b together with the theoretical dispersion curves and leaky mode velocities. The poor fitting of the coherences in Fig. 7 for frequencies up to ~ 0.9Hz confirms that $\rho_{1,2}$ (and G_{zz}) is not dominated by a unique horizontal velocity in that frequency band. Moreover, the mean horizontal velocities in this range grow steeply as frequency increases, from fundamental-mode Rayleigh-wave velocities (about 600m/s at 0.7Hz) to the leaky mode branch velocities of 975m/s at 0.9Hz (Fig. 6b). The shape of $\rho_{1,2}$ is well fitted by a Bessel function at f_P (1Hz for Model 1) indicating horizontal propagation of the energy.

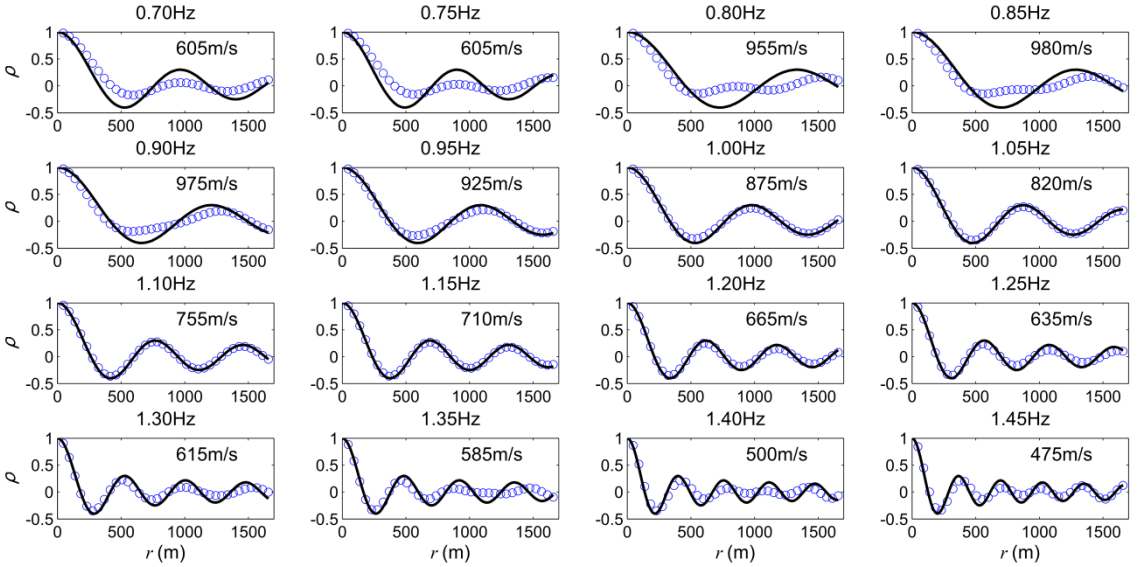

Figure 7. Full-wavefield calculation of $\rho_{1,2}(r)$ under the DFA (open circles) for Model 1 at frequencies around f_P. For each frequency (panel), the best fittings of $\rho_{1,2}(r)$ with a function $J_0(\omega r / c')$ is shown with black line and labeled with the apparent value of c'.

In this case, the retrieved velocity of 875m/s (green dot in Fig. 6b) matches perfectly the theoretical value for slowly-attenuating leaky waves obtained by solving $K = L = 0$ (Sections 2 and 3). The predominance of this guided wave is the consequence of the weak medium response of the fundamental Rayleigh mode at f_P (Fig 3e) and a negligible contribution of the branch-line integrals. The resemblance between $\rho_{1,2}$ and a $J_0(k'r)$ function is preserved at frequencies higher than f_P due to the significant fall in the medium response of the fundamental Rayleigh mode. Afterwards, the apparent velocity continues through the first higher mode, from its cut-off frequency (1.19Hz) up to about 1.3Hz, where it begins to return to the fundamental one with some loss of fitness of $\rho_{1,2}$ to the Bessel function.

5.2. Effects on the *f-k* spectrum

The *f-k* method (e.g. Lacoss *et al.* [15]) is another widely used algorithm for experimental analysis of propagation velocities of waves contained in ambient noise due its capability for resolving multiple velocities and usage with flexible array setups. To assess the detectability of the leaky modes and the slowly-attenuating leaky waves for the conventional *f-k* beam-forming power estimator P_{FKCV} in a simple yet representative case, we consider a centreless circular array with radius r composed of an odd number N_S of evenly spaced sensors. Ideally $P_{FKCV}(k,\varphi_k)$ should present peaks at wavenumbers k' and azimuths φ'_k coinciding with the characteristics of the energetic arrivals in the illuminating wavefield. Assuming that the wavefield is diffuse, the average of $P_{FKCV}(k,\varphi_k)$ over the observation directions φ_k will be (Appendix C)

$$\frac{\left\langle P_{FKCV}(k,\varphi_k)\right\rangle_{\varphi_k}}{\mathrm{N_S^2}} = \frac{cte}{\pi}\sum_{j=0}^{(\mathrm{N_S}-1)/2} \mathrm{Im}\,G_{zz}(2r\,|\sin\frac{\theta_j}{2}|)\;J_0(2kr\,|\sin\frac{\theta_j}{2}|)\Delta\theta - \frac{cte}{\mathrm{N_S}}\mathrm{Im}\,G_{zz}(0)\,, \quad (11)$$

where $\Delta\theta = 2\pi/\mathrm{N_S}$ and *cte* represents the frequency-dependent ratio between the power-spectrum of the vertical motion and the imaginary part of the Green's function at the source: $C_{jj} = cte \times \mathrm{Im}[G_{zz}(0;0)]$ (e.g., Sánchez-Sesma *et al.* [5]). Since the considered wavefield is azimuthally homogeneous, $P_{FKCV}(k,\varphi_k)$ will depend weakly on φ_k provided that $\mathrm{N_S}$ is large enough. For $\mathrm{N_S}$ tending to infinity, the sum in (11) turns into an integral between $\theta = 0$ and π, the term $-cte\,\mathrm{Im}\,G_{zz}(0)/\mathrm{N_S}$ vanishes and $P_{FKCV}(k,\varphi_k) = \left\langle P_{FKCV}(k,\varphi_k)\right\rangle_{\varphi_k}$.

Figure 8 shows the theoretical shape of $\left\langle P_{FKCV}\right\rangle_{\varphi_k}$ for Model 1 in a frequency band around f_p by using full wavefield computation for G_{zz}. $\mathrm{N_S}$ was fixed to 79 and the radius *r* of the virtual array was 834 m ($k_p r = 6$) in order to obtain enough resolution at long wavelengths (e. g., setting $kr > \pi$ is suggested for regular polygonal arrays by SESAME's [30] guidelines). The highest peak in $\left\langle P_{FKCV}\right\rangle_{\varphi_k}$ with $k' > \pi/r$ is identified at each frequency and used for computation of the main apparent horizontal phase velocity $c' = \omega/k'$. The results are shown in Fig. 9 with filled squares and compared with Rayleigh waves and leaky modes velocities. The secondary peaks of $\left\langle P_{FKCV}\right\rangle_{\varphi_k}$ discernible in Fig. 8 may either represent propagation of another seismic phase or be an effect of the limited performance of the beam-forming method or of the array settings (e.g., spatial aliasing). To investigate this fact, the curves have been compared with the theoretical shape when a single horizontal velocity exists, which correspond to assuming $\mathrm{Im}\left[G_{zz}(2r\sin\theta/2)\right] \propto J_0(2k'r\sin\theta/2)$ in Eq. (11), taking k' as the wavenumber of the main peak. A scale factor has been introduced to these curves (solid black lines in Fig. 8) to fit also the amplitude of the main peak. At those frequencies for which the second higher peak cannot be explained with the sole velocity c', the corresponding secondary wavenumber k'' has been picked. The secondary velocity $c'' = \omega/k''$ is also shown with open squares in Fig 9. As shown, these velocities match well the fundamental Rayleigh mode, the first higher mode or its continuation as a leaky mode.

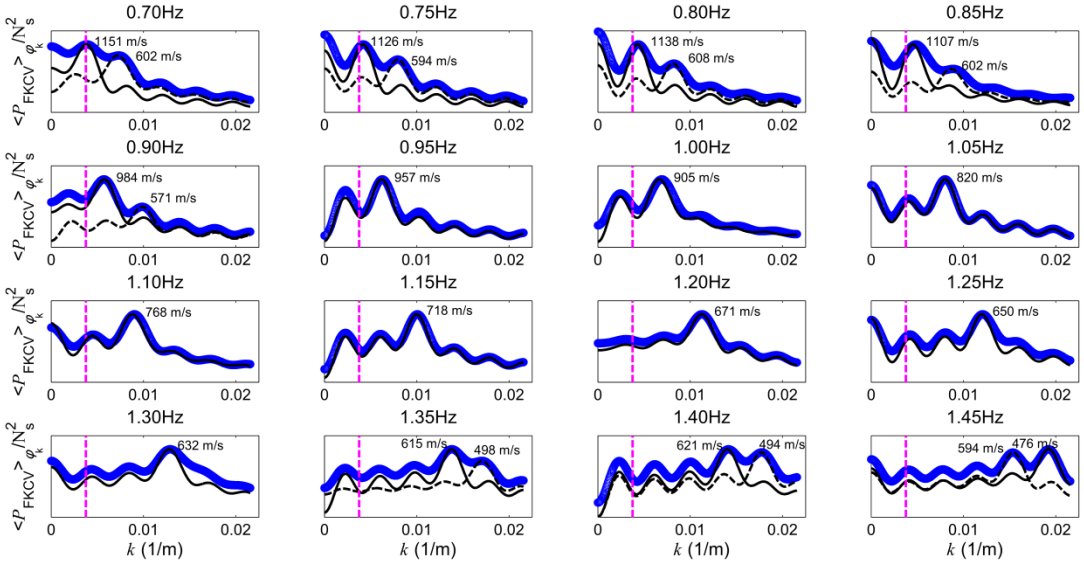

Figure 8. Synthetic azimuthally averaged $P_{FKCV}(\vec{k})$ spectra (blue lines) for the full wavefield after normalization by $G_{zz}(0;0;f)$. The rescaled theoretical values of $\left\langle P_{FKCV} \right\rangle_{\varphi_k}$ for the single horizontal velocity c' corresponding to the main peak are shown with solid black lines. The analogous functions for the second higher peaks are shown with dashed black lines whenever c' fails to reproduce the global shape of P_{FKCV}. Velocities c' and eventually c'' are displayed next to the corresponding peaks. Vertical dashed lines indicate the minimum reliable value of k, estimated as $k_{min}=\pi/r$. Model 1 in Table 1 and a regular polygonal array with r = 834 m and N_S = 79 were used in these computations.

The shape of $\left\langle P_{FKCV} \right\rangle_{\varphi_k}$ in the band from 0.95 to 1.25 Hz corresponds to a single phase velocity which matches well the first higher mode of Rayleigh waves or its continuation as a leaky mode branch (Fig. 9). Below 0.95 Hz, the full-wavefield *f-k* spectrum can be no longer explained from a well-defined velocity but it reflects as a mixture of waves with two different velocities, one corresponding to fundamental-mode Rayleigh waves (c ~ 600 m/s) and another to body waves, with c ranging from 980 m/s at 0.9 Hz up to 1550 m/s at 0.7 Hz, which can be accurately described in terms of leaky waves. The array radius used is too small to resolve frequencies below 0.7 Hz. An steep transition between these two patterns occurs near f_p. The fundamental mode becomes again perceptible at 1.35 Hz, with growing peak amplitudes as frequency increases. If the radius of the array is reduced to half (417 m), its resolution shifts toward higher frequencies and the *f-k* power estimator is able to follow the fundamental mode, which is the only relevant velocity up to about 3Hz (gray triangles in Fig. 9).

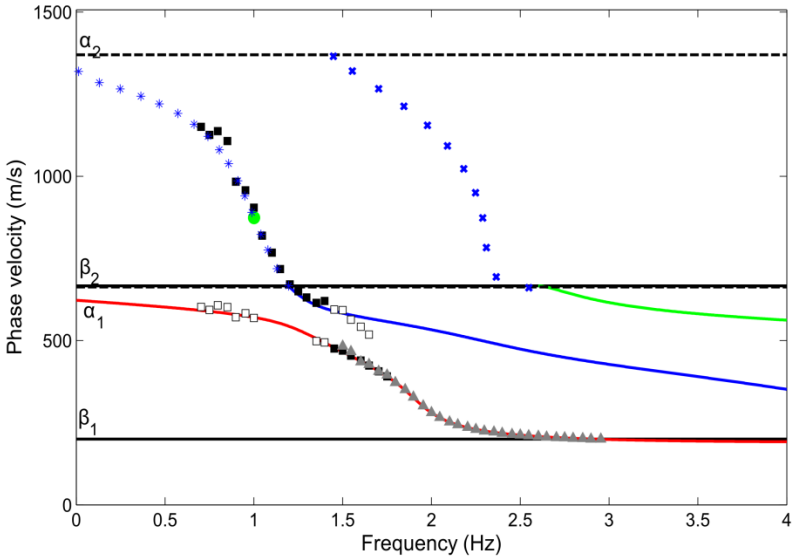

Figure 9. Apparent horizontal phase velocities obtained from *f-k* analysis as described in Fig. 8. Filled and open squares correspond to main peaks and secondary peaks in the *f-k* spectra. Triangles show results for a smaller array with r = 417 m. Rayleigh wave phase velocities (colored curves) and leaky mode (asterisks and crosses) for Model 1 are shown for reference.

6. Discussion

The synthetic example analyzed above shows predominant body wave propagation in the SPAC coefficient in a significant frequency band which spans from 0.7 f_{S0} to 1.2 f_{S0}. Their coexistence together with the fundamental Rayleigh mode is perceived in the f-k spectra in a broader band. This behavior contrasts with the dominance of the fundamental or higher modes of Rayleigh waves assumed in most of the recent works dealing with vertical-component ambient noise. The apparent horizontal velocities of these body-waves match well those of the leaky modes (Figs. 6b and 9), so that the contribution of the integrals along the branch-cuts shown in Fig. 3c appears to be negligible. At ω_p, these numerical experiments show that i) the coherence between vertical components vs. r fits well a $J_0(kr)$ function and ii) the *f-k* spectrum presents a clear peak, with the whole shape of $\left\langle P_{FKCV} \right\rangle_{\varphi_k}$ being reproducible by a sole horizontal velocity. The estimated phase velocity matches well the theoretical value of c_p determined in Section 4. These two observations, which fail at frequencies as close as $0.9\,\omega_p$, show that the wavefield at ω_p is dominated by the slowly-attenuating leaky waves studied here.

Many experimental studies have revealed deviations of the vertical-component ambient noise coherences from regular J_0-type shapes, i.e. from J_0 [2 π $s(f)$ f] relations with smoothly increasing horizontal slowness $s(f)=1/c(f)$. Low absolute coherences in broad frequency bands (usually below f_{S0}) may reveal poorly correlated signals due to electronic noise or attenuation. Nevertheless, features such as bumps, narrow picks or troughs should be interpreted in terms of the wavefield composition. Tokimatsu [3], Lunedei and Albarello [6] and Ohori [4], among others, described anomalies in the effective dispersion curves due to jumping between the fundamental mode and the first higher modes of Rayleigh waves from numerical or experimental approaches. If the

interstation distance is small enough, that perturbations are mapped into the first decreasing part of the SPAC coefficient at low-frequencies, where they are not masked by the Bessel function oscillations (e.g. Fig. 6a in Asten [28]). In contrast with the arguments given in those papers, the example in Section 5.1 (Fig. 6) demonstrates that full-wavefield calculations may be required to account for the bumps, which could be an effect of both body waves and higher surface wave modes in general cases. Recently, Chávez-García et al. [24] have studied small troughs or *loss of correlation* found in narrow bands around the local f_{S0} in a collection of experimental ambient noise coherences. Our results suggest an interpretation in terms of incremented coherences in a band above f_{S0} due to coexistence of the mentioned faster propagation modes. This is preferable to assuming an actual drop in the fundamental mode correlation due to poor signal-noise ratios which are not fully supported by the experiments.

Bonnefoy-Claudet *et al.* [23] [31], performed *f-k* analysis of synthetic ambient noise wavefields, paying special attention to their composition around f_{S0} and its harmonics. The horizontal phase velocity derived from their virtual array experiment in [23] showed sharp increments around f_{S0} which were interpreted as effects of poor performance of the *f-k* method. The elastic version of the structure used, consisting of a soft layer over a halfspace, has been listed in Table 1 (Model 2). In that case, a zero in F_R at 1.921Hz (f_p / f_{S0} = 0.961) results from procedure described in Section 4. It corresponds to a phase velocity of 1354m/s (larger than β_2 = 1000 m/s). P waves in the layer are of homogeneous type at that frequency though they spread almost horizontally (86º incidence angle on the interfaces). Even though larger array apertures would be recommendable for accurate analysis, the effect of guided waves with slow amplitude decay is probably behind their results.

7. Conclusions

Numerical calculations in simple layered models (e.g., Tamura [2]) showed that guided P-SV body waves may represent an important component of the Green function between surface source and receiver in particular frequency bands. The energy of these waves decay as slowly as surface waves for increasing distances, so that they remain detectable far away from the sources. In this paper we have explored the striking similarity between the P-SV wave-system and Rayleigh waves at some particular frequencies ω_p fulfilling $K = L = 0$. These waves correspond to isolated points in the leaky mode path at which $k_p = k(\omega_p)$ become real, with a phase velocity $c_p = \omega_p / k_p$ faster than S waves in the halfspace. The contributions of these zeros of $F_R(\omega,k)$ presents several Rayleigh wave characteristics, such as real Harkrider's medium responses, $\pi/2$ phase lags between horizontal and vertical components and $\sim r^{-1/2}$ decay of amplitudes with distance, instead of the $r^{-1/2}$ exp[−Im(k) r] decreasing of regular leaky waves. The cancellation of the homogeneous downgoing S wave at ω_p implies that the wavefield in the halfspace consists of an inhomogeneous P wave only, unlike surface waves.

The existence and the frequency of these waves have been investigated for models consisting of a layer with moderate to high velocity contrasts with a stiffer halfspace. For the fixed ν_2 and density contrast used by Tuan *et al.* [21] and usual Poisson's ratios ν_1 in the layer from 0.25 to 0.49, S wave velocity contrasts larger than 2.16 - 2.48 are required. In these cases, a pole with the mentioned characteristics appears close to f_{S0},

with maximum deviations from that value of -5% and +30%. A similar range for f_p has been found if ν_2 is varied instead of ν_1, though much larger negative deviations from f_{S0} appear for very low values of ν_2.

We have studied the perturbations induced by these guided waves in two methods of experimental estimation of phase velocities in stochastic wavefields based on coherence measurements. For this purpose, a simple profile presenting slowly attenuating leaky waves has been considered along with the validity of the DFA, taking all the propagation modes into account. The numerical simulations for an example model with high velocity contrast (3.3 for S waves) clearly point to the detectability of these waves around f_{S0} in both the SPAC coefficient and the f-k power spectrum. These results provide additional insight into the composition of the ambient noise around the S wave resonance frequencies.

Another important aspect of this issue lies in the sensitivity of the particle trajectory and amplitude of motion around f_{S0} to the main S wave velocity contrasts in the underground structure. Even though it is a controversial topic, the interpretation of these trajectories under ambient noise illumination is the basis of several tools for estimation of local amplifications of seismic signals and methods for passive seismic exploration (e.g., Nakamura [7], Lachet and Bard [32], García-Jerez *et al.* [33],[34], Fäh *et al.* [35], Arai and Tokimatsu [36], Parolai *et al*. [37], Herak [38], Sánchez-Sesma *et al*. [39], Tuan *et al.* [21]). Though further research is required, our results point to a major role of the leaky modes and guided waves in the in-plane particle trajectories in that frequency band.

Finally, it is also worth noting that the pole in the P-SV integrand associated with these waves may lead to instability in numerical calculations of the Green's functions at frequencies around ω_p whenever the integration contour shown in Fig. 2 (or that in Wang and Herrmann [12]) is used. Rerouting the branch-cuts when the Green's function is calculated at frequencies around ω_p would be the preferred procedure. On the other hand, numerical artifices which attempt to remove the poles from the real k by adding a tunable imaginary perturbation to the frequency (Bouchon and Aki [11], Herrmann and Ammon [40]) also provide suitable approximate solutions.

Acknowledgements

The authors thank Prof. Boris Gurevich and Prof. Boris Kashtan for their constructive comments. We especially thank Prof. Francisco Luzón for careful reading and fruitful discussions. This research work was partially supported by the Spanish Comisión Interministerial de Ciencia y Tecnología projects CGL2010-16250, CGL2011-29499-C02-01 and CGL2011-30187-C02-02, the European Union with Fondo Europeo de Desarrollo Regional, the DGAPA-UAM under Project IN104712 and the AXA Research Fund. The work done by A. G.-J. was under Juan de la Cierva contract at Instituto Andaluz de Geofísica, Universidad de Granada, Spain.

References

[1] K. Konno, T. Ohmachi, Ground-Motion Characteristics Estimated from Spectral Ratio between Horizontal and Vertical Components of Microtremor, Bull. Seismol. Soc. Am. 88 (1998) 228-241.

[2] S. Tamura, Comparison of Body and Rayleigh Wave Displacements Generated by a Vertical Force on a Layered Elastic Medium, in: Proc. 11th World Conf. on Earthquake Engineering, 1996, paper 1722.
[3] K. Tokimatsu, Geotechnical site characterization using surface waves, in: Ishihara (Ed.), Earthquake Geotechnical Engineering, Balkema, Rótterdam, 1997, pp. 1333-1368.
[4] M. Ohori, A. Nobata, K. Wakamatsu, A comparison of ESAC and FK methods of estimating phase velocity using arbitrarily shaped microtremor arrays, Bull. Seismol. Soc. Am. 92 (2002) 2323-2332.
[5] F.J. Sánchez-Sesma, J.A. Pérez-Ruiz, F. Luzón, M. Campillo, A. Rodríguez-Castellanos, Diffuse fields in dynamic elasticity, Wave Motion 45 (2008) 641–654.
[6] E. Lunedei, D. Albarello, On the seismic noise wavefield in a weakly dissipative layered Earth, Geophys. J. Int. 177 (2009) 1001–1014.
[7] Y. Nakamura, A method for dynamic characteristics estimations of subsurface using microtremors on the ground surface, Q. Rept. RTRI Jpn. 30 (1989) 25-33.
[8] F. Gilbert, Propagation of transient leaking modes in a stratified elastic waveguide, Rev. Geophys. 2 (1964) 123-152.
[9] W.M. Ewing, W.S. Jardetsky, F. Press, Elastic Waves in Layered Media, McGraw-Hill Book Co., New York, 1957.
[10] R.A.W. Haddon, Computation of synthetic seismograms in layered earth models using leaking modes, Bull. Seismol. Soc. Am. 74 (1984) 1225-1248.
[11] M. Bouchon, K. Aki, Discrete wave-number representation of seismic-source wave fields, Bull. Seismol. Soc. Am. 67 (1977) 259-277.
[12] C.Y. Wang, R.B. Herrmann, A numerical study of P-, SV-, and SH-wave generation in a plane layered medium, Bull. Seismol. Soc. Am. 70 (1980) 1015-1036.
[13] A. Ben-Menahem, S. J. Singh, Seismic waves and sources, second ed., Dover, New York, 2000.
[14] K. Aki, Space and time spectra of stationary stochastic waves, with special reference to microtremors, Bulletin of the Earthquake Research Institute 35 (1957) 415–456.
[15] R.T. Lacoss, E.J. Kelly, T.M. Nafi, Estimation of seismic noise structure using arrays, Geophysics 34 (1969) 21–38.
[16] D.G. Harkrider, Surface waves in multilayered elastic media. Part 1, Bull. Seismol. Soc. Am. 54 (1964) 627-679.
[17] N.A. Haskell, The dispersion of surface waves on multilayered media, Bull. Seismol. Soc. Am. 43 (1953) 17-34.
[18] T.H. Watson, A Real Frequency, Complex Wave-Number Analysis of Leaking Modes, Bull. Seismol. Soc. Am. 62 (1972) 369-384.
[19] S.J. Laster, J.G. Foreman, A.F. Linville, Theoretical investigation of modal seismograms for a layer over a half-space, Geophysics 30 (1965) 571-596.
[20] Y.A. Surkov, V.V. Reshetnikov, Numerical Study of Properties of Quasilocal Plane Waves of the Modal Type in the Case of a Thin Low-Velocity Layer that is in Contact with an Elastic Half-Space, Journal of Mathematical Sciences 132 (2006) 103-112.
[21] T.T. Tuan, F. Scherbaum, P.G. Malischewsky, On the relationship of peaks and troughs of the ellipticity (H/V) of Rayleigh waves and the transmission response of single layer over half-space models, Geophys. J. Int. 184 (2011) 793-800.
[22] B. Endrun, Love wave contribution to the ambient vibration H/V amplitude peak observed by array measurements, Journal of Seismology 15 (2011) 443-472.
[23] S. Bonnefoy-Claudet, C. Cornou, P-Y. Bard, F. Cotton, P. Moczo, J. Kristek, D.

Fäh, H/V ratio: a tool for site effects evaluation. Results from 1-D noise simulations, Geophys. J. Int. 167 (2006) 827-837.
[24] F.J. Chávez-García, M.V. Manakou, D.G. Raptakis, Subsoil structure and site effects: A comparison between results from SPAC and HVSR in sites of complex geology, Soil Dynamics and Earthquake Engineering 57 (2014) 133–142.
[25] N.M. Shapiro, M. Campillo, Emergence of broadband Rayleigh waves from correlations of the ambient seismic noise, Geophys. Res. Lett. 31 (2004) L07614, doi 10.1029/2004GL019491.
[26] T. Yokoi, S. Margaryan, Consistency of the spatial autocorrelation method with seismic interferometry and its consequence, Geophysical Prospecting 56 (2008) 435–451.
[27] J. Roberts, M. Asten, H.H. Tsang, S. Venkatesan, N. Lam, Shear Wave Velocity Profiling in Melbourne Silurian Mudstone Using the SPAC Method, in: Proc. AEES Conference at Mount Gambier, South Australia, 2004.
[28] M.W. Asten, Site shear velocity profile interpretation from microtremor array data by direct fitting of SPAC curves, in: Proc. Third International Symposium on the Effects of Surface Geology on Seismic Motion, Grenoble, France, 2006, Paper 99.
[29] T. Ikeda, T. Matsuoka, T. Tsuji, K. Hayashi, Multimode inversion with amplitude response of surface waves in the spatial autocorrelation method, Geophys. J. Int. 190 (2012) 541-552.
[30] SESAME, Report on FK/SPAC Capabilities and Limitations. WP06 - Derivation of dispersion curves, SESAME-Project (EVG1-CT-2000-00026), Report-Nr. D19.06, 2005.
[31] S. Bonnefoy-Claudet, A. Köhler, C. Cornou, M. Wathelet, P.-Y. Bard, Effects of Love Waves on Microtremor H/V Ratio, Bull. Seismol. Soc. Am. 98 (2008) 288 - 300.
[32] C. Lachet, P.Y. Bard, Numerical and Theoretical Investigations on the Possibilities and Limitations of Nakamura's Technique, Journal of Physics of the Earth 42 (1994) 377-397.
[33] A. García-Jerez, F. Luzón, M. Navarro, J.A. Pérez-Ruíz, Characterization of the sedimentary cover of the Zafarraya basin (Southern Spain) by means of ambient noise, Bull. Seismol. Soc. Am. 96 (2006) 957-967.
[34] A. García-Jerez, F. Luzón, F.J. Sánchez-Sesma, E. Lunedei, D. Albarello, M.A. Santoyo, J. Almendros, Diffuse elastic wavefield within a simple crustal model. Some consequences for low and high frequencies, J. Geophys. Res. 118 (2013) 5577–5595.
[35] D. Fäh, F. Kind, D. Giardini, Inversion of local S-wave velocity structures from average H/V ratios and their use for the estimation of site-effects, Journal of Seismology 7 (2003) 449-467.
[36] H. Arai, K. Tokimatsu, S-wave velocity profiling by inversion of microtremor H/V spectrum, Bull. Seism. Soc. Am. 94 (2004) 53-63.
[37] S. Parolai, M. Picozzi, S.M. Richwalski, C. Milkereit, Joint inversion of phase velocity dispersion and H/V ratio curves from seismic noise recordings using a genetic algorithm, considering higher modes, Geophys. Res. Lett. 32 (2005) L01303, doi:10.1029/2004GL021115.
[38] M. Herak, ModelHVSR - A Matlab® Tool to Model Horizontal-to-Vertical Spectral Ratio of Ambient Noise, Computers & Geosciences 34 (2008) 1514–1526.
[39] F.J. Sánchez-Sesma, M. Rodríguez, U. Iturrarán-Viveros, F. Luzón, M. Campillo, L. Margerin, A. García-Jerez, M. Suarez, M.A. Santoyo, A. Rodríguez-Castellanos, A theory for microtremor H/V spectral ratio: application for a layered medium, Geophys. J. Int. 186 (2011) 221-225.
[40] R.B. Herrmann, C.J. Ammon, Computer programs in seismology, an overview of

synthetic seismogram computation, St. Louis Univ., St. Louis Mo., 2003.

Appendix A

In this Appendix we study the consequences of the simultaneous fulfillment of the equations $K = 0$ and $L = 0$ at a particular combination (ω_p, k_p).

The P-SV Green functions can be written in terms of elements of the matrix **J**, defined as the product $\mathbf{E}_N^{-1}\mathbf{A}$, where **A** represents the product of layer matrices and $\mathbf{E}_N^{-1}$ depends on the halfspace properties (apart from *k* and *c*). Their expressions can be found in Ben-Menahem and Singh [13], Eqs. 3.184, 3.185 and 3.190c. For $\beta_N < c < \alpha_N$, elements of **J** are real (*R*) or imaginary (*I*) following:

$$\mathbf{J} = \begin{pmatrix} R & I & R & I \\ R & I & R & I \\ R & I & R & I \\ I & R & I & R \end{pmatrix}. \tag{A1}$$

Matrix **J** provides a link between the upgoing/downgoing P and S wave amplitudes at the halfspace (or their inhomogeneous counterparts) and the displacement-stress vector at surface. If neither upgoing homogeneous waves nor unbounded inhomogeneous waves are permitted at the halfspace, this relationship is written

$$\begin{pmatrix} P & P & S & S \end{pmatrix}^T = \mathbf{J} \begin{pmatrix} \dot{u}/c & \dot{w}/c & 0 & 0 \end{pmatrix}^T, \tag{A2}$$

where *P* and *S* are proportional to the respective amplitudes of the allowed waves at halfspace (downgoing waves or exponentially decaying amplitudes).

Harkrider's expressions of the Green's functions are written in terms of the quantities *M*, *N*, *K*, *L*, *R*, *S*, *G*, *H* which are proportional to differences between pairs of elements of **J,** e.g., $K = (J_{22} - J_{12})\alpha_N^2 \eta_{\alpha_N} / c^2$ and $L = -(J_{11} - J_{21})\alpha_N^2 \eta_{\alpha_N} / c^2$, being mutually linked by the relationship $R\,N - S\,L = G\,M - H\,K$ (Harkrider [16], Eqs. 68 – 69). In the case considered here ($K = L = 0$), this general property simply reads $R\,N = G\,M$, or equivalently, $(J_{14} - J_{24})(J_{31} - J_{41}) = (J_{13} - J_{23})(J_{32} - J_{42})$. Considering now (A1), both sides of this latter expression will be complex quantities, so that, it can be separated in simultaneous conditions for the real and imaginary parts:

$$J_{31}(J_{14} - J_{24}) - J_{32}(J_{13} - J_{23}) = 0 \tag{A3a}$$

$$J_{41}(J_{14} - J_{24}) - J_{42}(J_{13} - J_{23}) = 0. \tag{A3b}$$

The trivial solution of this system, $(J_{14} - J_{24}) = (J_{13} - J_{23}) = 0$ along with $K = L = 0$ implies that **J** is singular ($J_{1j} = J_{2j}$ for any *j*). Disregarding that case, the compatibility between Eqs. (A3) would require:

$$J_{31}J_{42} = J_{32}J_{41}\ . \tag{A4}$$

This property, together with the third and fourth equations in (A2), yields $S = 0$ and

$$\dot{u}/\dot{w} = -M/N = -J_{32}/J_{31} = -J_{42}/J_{41} \in \Im, \tag{A5}$$

implying existence of pure P- type inhomogeneous waves in the halfspace and elliptic particle motion at surface, respectively.

The excitation of this vibration mode by a surface point load can be evaluated as the residue contribution of integrals (1-4) at (ω_p, k_p). Using the Harkrider's *medium response* A_{ω_p,k_p} defined as $2\pi i$ times the residue of $g_{zz}(\omega,k,0)/F_R$ at (ω_p, k_p), where $g_{zz}(\omega,k,0)$ correspond to $[LH - GN]/(2\pi)$ and

$$G = \gamma_{\mathrm{N}}\eta_{\alpha_{\mathrm{N}}}\mathrm{A}_{13} + (\gamma_{\mathrm{N}} - 1)\mathrm{A}_{23} - \frac{\eta_{\alpha_{\mathrm{N}}}\mathrm{A}_{33} - \mathrm{A}_{43}}{\rho_{\mathrm{N}}c^2}, \tag{A6}$$

$$H = -(\gamma_{\mathrm{N}} - 1)\mathrm{A}_{13} + \gamma_{\mathrm{N}}\eta_{\beta_{\mathrm{N}}}\mathrm{A}_{23} + \frac{\mathrm{A}_{33} + \eta_{\beta_{\mathrm{N}}}\mathrm{A}_{43}}{\rho_{\mathrm{N}}c^2}, \tag{A7}$$

and using that K, L tend to zero as $k \to k_p$ we can obtain:

$$A_{\omega_p,k_p} = \frac{iG}{(M/N)(\partial L/\partial k)_{\omega_p} - (\partial K/\partial k)_{\omega_p}}\ . \tag{A8}$$

Appendix B

A way for resolution of the system of equations $K(k, c) = 0$, $L(k, c) = 0$ for a single layer over a halfspace is proposed below. The expressions of K and L for N = 2 are (Eq. 3.200 in Ben-Menahem and Singh [13]):

$$K = (J_{22} - J_{12})\alpha_2^2\eta_{\alpha_2}/c^2 = \gamma_2\eta_{\alpha_2}\mathrm{A}_{12} + (\gamma_2 - 1)\mathrm{A}_{22} - \frac{\eta_{\alpha_2}\mathrm{A}_{32} - \mathrm{A}_{42}}{\rho_2 c^2} \tag{B1}$$

$$L = -(\mathrm{J}_{11} - \mathrm{J}_{21})\alpha_2^2\eta_{\alpha_2}/c^2 = \gamma_2\eta_{\alpha_2}\mathrm{A}_{11} + (\gamma_2 - 1)\mathrm{A}_{21} - \frac{\eta_{\alpha_2}\mathrm{A}_{31} - \mathrm{A}_{41}}{\rho_2 c^2} \tag{B2}$$

where **A** represents the layer matrix. Replacing the expressions of the elements of **A** (Eq. 3.185 in Ben-Menahem and Singh [13], we can rewrite these equations, respectively, in the form:

$$\mathrm{A}_{\mathrm{K}}\sin P + \mathrm{B}_{\mathrm{K}}\cos P + \mathrm{C}_{\mathrm{K}}\sin Q + \mathrm{D}_{\mathrm{K}}\cos Q = 0 \tag{B3}$$

$$\mathrm{A}_{\mathrm{L}}\sin P + \mathrm{B}_{\mathrm{L}}\cos P + \mathrm{C}_{\mathrm{L}}\sin Q + \mathrm{D}_{\mathrm{L}}\cos Q = 0 \tag{B4}$$

with $Q = k\eta_{\beta_1} h$ and $P = k\eta_{\alpha_1} h$. Hereafter, A_K, B_K, C_K, D_K, A_L, B_L, C_L and D_L are considered as functions of *c* (not depending on *k*). Writing now $\sin P$ and $\cos P$ as functions of the half-angle $P_h = P/2$, and after a multiplication by $1+\tan^2 P_h$, it yields

$$(-B_K + D_K \cos Q + C_K \sin Q)\tan^2 P_h + 2A_K \tan P_h + (B_K + D_K \cos Q + C_K \sin Q) = 0 \quad \text{(B5)}$$

$$(-B_L + D_L \cos Q + C_L \sin Q)\tan^2 P_h + 2A_L \tan P_h + (B_L + D_L \cos Q + C_L \sin Q) = 0 \quad \text{(B6)}$$

At this point, $\tan P_h$ can be worked out for both the equations:

$$\tan P_h = \frac{-A_K + sg_K \sqrt{A_K^2 - (-B_K + D_K \cos Q + C_K \sin Q)(B_K + D_K \cos Q + C_K \sin Q)}}{-B_K + D_K \cos Q + C_K \sin Q} \quad \text{(B7)}$$

$$\tan P_h = \frac{-A_L + sg_L \sqrt{A_L^2 - (-B_L + D_L \cos Q + C_L \sin Q)(B_L + D_L \cos Q + C_L \sin Q)}}{-B_L + D_L \cos Q + C_L \sin Q}, \quad \text{(B8)}$$

and equaling their expressions we obtain

$$\begin{aligned} &\frac{A_L}{-B_L + D_L \cos Q + C_L \sin Q} - \frac{A_K}{-B_K + D_K \cos Q + C_K \sin Q} + \\ &\frac{sg_K \sqrt{A_K^2 - (-B_K + D_K \cos Q + C_K \sin Q)(B_K + D_K \cos Q + C_K \sin Q)}}{-B_K + D_K \cos Q + C_K \sin Q} \\ &- \frac{sg_L \sqrt{A_L^2 - (-B_L + D_L \cos Q + C_L \sin Q)(B_L + D_L \cos Q + C_L \sin Q)}}{-B_L + D_L \cos Q + C_L \sin Q} = 0 \end{aligned} \quad \text{(B9)}$$

Removing square roots and after some algebra, an expression which depends on Q via $\cos^2 Q$, $\sin^2 Q$ and $\sin Q \cos Q$ is obtained. Using the identities $\cos^2 Q = 1/(1+\tan^2 Q)$, $\sin^2 Q = \tan^2 Q/(1+\tan^2 Q)$, $\sin Q \cos Q = \tan Q/(1+\tan^2 Q)$, (B9) can be rewritten as a quadratic equation in $t\tan Q$:

$$X\, t\tan^2 Q + 2Y\, t\tan Q + Z = 0 \quad \text{(B10)}$$

where the depending of *c* coefficients are:

$$X = A_K^2 (C_L^2 - B_L^2) + A_L^2 (C_K^2 - B_K^2) + (B_L C_K - B_K C_L)^2 + 2A_K A_L (B_K B_L + C_K C_L),$$

$$Y = C_K D_K (A_L^2 + B_L^2) + C_L D_L (A_K^2 + B_K^2) - (A_K A_L + B_K B_L)(C_L D_K - C_K D_L),$$

$$Z = A_L^2\,(-B_K^2 + D_K^2) + (B_L\,D_K - B_K\,D_L)^2 + 2\,A_K\,A_L\,(B_K\,B_L - D_K\,D_L) + A_K^2\,(-B_L^2 + D_L^2)$$

.

Thus, two solutions are obtained for $\tan Q$ corresponding to the sign of the root (say sg_{TQ}) and, for each one, a set of solutions for the wavenumber $k_{sg_{TQ},n} = (Q_{sg_{TQ}} + n\pi)/(r_{\beta_1} h)$, with $0 \le Q_{sg_{TQ}} < \pi$. This solutions fulfill (B9) for unknown signs sg_K, sg_L. Finally, sg_K or sg_L are determined and $k_{sg_{TQ},n}(c)$ is replaced in (B7) or (B8) to search for numerical solutions of c for each couple (n, sg_{TQ}).

Appendix C

A brief derivation of the conventional *f-k* power estimator P_{FKCV} under DFA for a dense circular array is listed below.

The definition of P_{FKCV} for any array consisting of N_S stations at $\vec{r}_j$, j = 0, 1,…, N_S–1 is:

$$P_{FKCV}(\vec{k}) = \sum_{j,l=0}^{N_S-1} C_{jl} \exp[i\,\vec{k}(\vec{r}_j - \vec{r}_l)]\,. \qquad \text{(C1)}$$

Then, assuming that the stations are evenly located on a circumference with radius r, we can define the azimuth of the station at $\vec{r}_j$ as $\theta_j = j2\pi / N_S$. For a diffuse wavefield the relation $C_{jl} = cte\,\mathrm{Im}G_{zz}(|\vec{r}_l - \vec{r}_j|)$ holds. Thus, defining (k, φ_k) as the modulus and azimuth of the investigated wavenumber $\vec{k}$ and using elemental trigonometry, (C1) yields:

$$\frac{P_{FKCV}(\vec{k})}{N_S^2} = \frac{cte}{N_S^2} \sum_{j,l=0}^{N_S-1} \mathrm{Im}G_{zz}(2r\,|\sin\frac{\theta_j - \theta_l}{2}|) \exp\{i\,kr[\cos(\theta_j - \varphi_k) - \cos(\theta_l - \varphi_k)]\}\,. \qquad \text{(C2)}$$

After some elementary manipulations and summing once for each pair of sensor, equation (C2) reads

$$\frac{P_{FKCV}(\vec{k})}{N_S^2} = \frac{2cte}{N_S^2} \sum_{\substack{j,l=0 \\ j \ge l}}^{N_S-1} \mathrm{Im}G_{zz}(2r\,|\sin\frac{\theta_j - \theta_l}{2}|) \cos[2kr\sin(\frac{\theta_j + \theta_l}{2} - \varphi_k)\sin(\frac{\theta_j - \theta_l}{2})]$$

$$- \frac{cte}{N_S^2} \sum_{j=1}^{N_S} \mathrm{Im}G_{zz}(0)\,, \qquad \text{(C3)}$$

which, after taking the mean value over the observation azimuth φ_k yields

$$\frac{\langle P_{FKCV}\rangle_{\varphi_k}}{N_S^2}=\frac{2cte}{N_S^2}\sum_{\substack{j,l=0\\ j\geq l}}^{N_S-1}\mathrm{Im}\,G_{zz}(2r|\sin\frac{\theta_j-\theta_l}{2}|)\,J_0(2kr|\sin\frac{\theta_j-\theta_l}{2}|)-\frac{cte}{N_S}\mathrm{Im}\,G_{zz}(0),\quad\text{(C4)}$$

with $\langle P_{FKCV}\rangle_{\varphi_k}$ depending on k. Assuming, for simplicity, that N_S is odd, every interstation distance $|2r\sin[(\theta_j-\theta_l)/2]|$ will appear N_S times in the sum. All these possible distances can be generated fixing index l to 0, and letting j run up to $(N_S-1)/2$:

$$\frac{\langle P_{FKCV}\rangle_{\varphi_k}}{N_S^2}=\frac{cte}{\pi}\sum_{j=0}^{(N_S-1)/2}\frac{2\pi}{N_S}\mathrm{Im}\,G_{zz}(2r|\sin\frac{\theta_j}{2}|)\,J_0(2kr|\sin\frac{\theta_j}{2}|)-\frac{cte}{N_S}\mathrm{Im}\,G_{zz}(0),\qquad\text{(C5)}$$

which corresponds to Eq. (11). If the number of sensors were very large (N_S tending to infinity), (C5) can be immediately written as

$$\frac{\langle P_{FKCV}\rangle_{\varphi_k}}{N_S^2}\to\frac{cte}{\pi}\int_0^{\pi}\mathrm{Im}\left[G_{zz}(2r\sin\frac{\theta}{2})\right]J_0(2kr\sin\frac{\theta}{2})d\theta.\qquad\text{(C6)}$$

At this limit, $P_{FKCV}(\vec{k})$ become independent of the direction of $\vec{k}$ so that Eq. (C6) could be derived without performing any previous average over φ_k.